



Annual Review of Marine Science

The Arctic Ocean's Beaufort Gyre

Mary-Louise Timmermans¹ and John M. Toole²

¹Department of Earth and Planetary Sciences, Yale University, New Haven, Connecticut, USA;
email: mary-louise.timmermans@yale.edu

²Department of Physical Oceanography, Woods Hole Oceanographic Institution, Woods Hole,
Massachusetts, USA

Annu. Rev. Mar. Sci. 2023. 15:6.1–6.26

The *Annual Review of Marine Science* is online at
marine.annualreviews.org

<https://doi.org/10.1146/annurev-marine-032122-012034>

Copyright © 2023 by the author(s).
All rights reserved

Keywords

Arctic Ocean, Beaufort Gyre, circulation, sea ice, freshwater, ocean heat content

Abstract

The Arctic Ocean's Beaufort Gyre is a dominant feature of the Arctic system, a prominent indicator of climate change, and possibly a control factor for high-latitude climate. The state of knowledge of the wind-driven Beaufort Gyre is reviewed here, including its forcing, relationship to sea-ice cover, source waters, circulation, and energetics. Recent decades have seen pronounced change in all elements of the Beaufort Gyre system. Sea-ice losses have accompanied an intensification of the gyre circulation and increasing heat and freshwater content. Present understanding of these changes is evaluated, and time series of heat and freshwater content are updated to include the most recent observations.



1. INTRODUCTION

The Arctic Ocean along with its sea-ice cover has a central role in global climate. Situated at the northern terminus of the atmospheric flows that transport heat and moisture poleward, this ocean receives a disproportionate amount by area of the global freshwater flux to the ocean through net precipitation and river runoff. The Arctic is a link between the Pacific and Atlantic Oceans, through which water circulates, transporting mass, heat, salt, nutrients, and organisms. A distinguishing feature of the Arctic Ocean, and one that allows for the formation and persistence of sea ice, is its halocline stratification, characterized by fresher, low-density waters overlying saltier, denser waters. Spatial variations in this stratification manifest a complex ocean circulation driven by the dynamic wind, as well as heat and freshwater forcing, under coastline and bathymetric constraints and sea-ice dynamics. Embedded in this complexity is the Beaufort Gyre (BG), one of the major circulation features of the Arctic Ocean.

1.1. Geographical Setting and Circulation

The wind-driven BG, a clockwise, surface-intensified circulation system centered over the abyssal plain of the Canada Basin (Figure 1), is the focus of this review. The BG may be characterized by its circulation and distinct temperature and salinity structure. While its center and horizontal extent can vary on seasonal, interannual, and decadal timescales, it is useful to introduce its broad domain in terms of geographic boundaries, which play an integral role in its structure and dynamics.

At its southern boundary are the Beaufort and Chukchi shelves off the coast of Canada and Alaska. The northern Chukchi Sea (over the Chukchi shelf) marks the southwest boundary of the

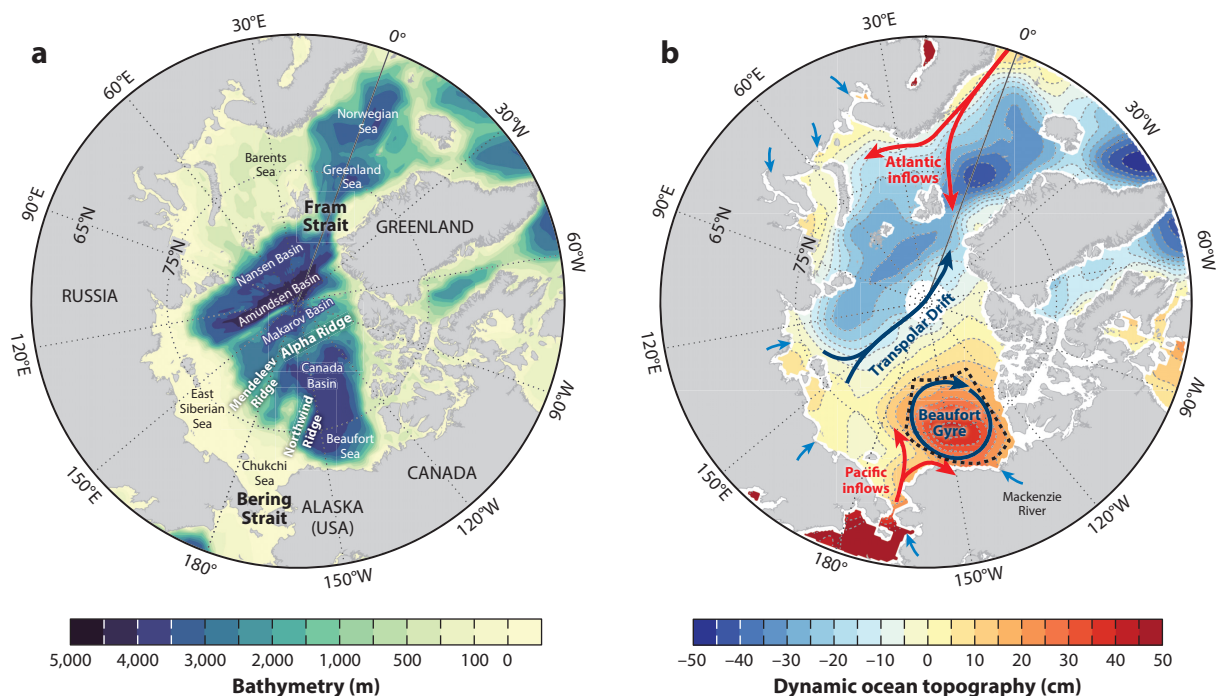


Figure 1

(a) Arctic Ocean basins, marginal seas, bathymetry (colors), and connecting straits integral to the Beaufort Gyre system. (b) Dynamic ocean topography (colors) averaged over the period 2003–2014 (Armitage et al. 2016, 2017), with schematic arrows indicating the primary circulation features that are imprinted in the field. The black dotted line bounds the Beaufort Gyre region.

6.2 Timmermans • Toole



BG. To the east lies the Canadian Arctic Archipelago, with straits that are transport pathways from the BG region to the subpolar North Atlantic. Extending northward from the Chukchi shelf region is the Chukchi Borderland region, with the Northwind Ridge on its eastern flank. This ridge often marks the western boundary of the BG, although a dynamic ocean topography characterization of its western extent suggests that the BG can at times extend far west of the Northwind Ridge, well into the Chukchi Borderland region (Regan et al. 2019). The Alpha Ridge bounding the Canada Basin to the north might be adopted as a reasonable approximation for the northern extent of the BG.

The imprint of the BG circulation in context with the major circulation features of the Arctic Ocean is clearly evident in the pan-Arctic pattern of mean dynamic ocean topography; geostrophic flow may be inferred from lateral gradients in dynamic ocean topography (**Figure 1b**). The highest dynamic heights in the Arctic Ocean mark the center of the anticyclonic BG. To its north, the gradient to lower dynamic height, with its axis approximately aligned from Siberia to Greenland, is associated with the wind-driven Transpolar Drift, which carries water and sea ice from the Siberian shelves across the Arctic Ocean toward Fram Strait. In general, a large-scale cyclonic circulation is present in the Eurasian Basin. To the south of Fram Strait, the cyclonic Greenland Gyre is marked by low dynamic height, with the northward-directed North Atlantic Current to its east.

1.2. Climate Context for the Beaufort Gyre

The surface-intensified ocean flow influences and is in turn influenced by the sea-ice cover, and it includes a component that accumulates and stores water that is relatively fresh compared with water in most other Arctic Ocean regions. For the same reason that it constitutes a freshwater reservoir, the BG accumulates and stores significant quantities of ocean heat in the form of warm-water layers found year-round at depth in the BG. The notable sea-ice decline in recent decades is spatially variable, with the Chukchi Sea and BG sector experiencing the largest losses (Liu et al. 2021). Sea-ice decline has made way for increased solar energy absorption by the surface ocean, freshwater accumulation and stratification anomalies, and changes in the seasonally varying momentum exchanges between the atmosphere and ocean. Each of these has important consequences for ocean dynamics, feedbacks to the sea-ice cover, and ecosystems within the Arctic.

Beyond the Arctic Ocean, it has been put forward that freshwater export from the BG to the North Atlantic may at times be of sufficiently high volume to influence global climate. For example, freshening in the North Atlantic associated with freshwater release from the Arctic Ocean has been purported to inhibit deep wintertime convection, which in turn may reduce the ocean overturning circulation (e.g., Vellinga et al. 2008, Zhang et al. 2021). Whether the influence is local to the Arctic or global, continued change involving the BG will have important consequences for global climate in the years and decades ahead.

In this review, we outline and explore the properties and dynamics of the large-scale BG, from its atmospheric driving to its sea ice and through its system of ocean layers; appraise present understanding of how the system works; highlight recent physical changes in the BG; and identify gaps in our understanding.

2. ATMOSPHERIC FORCING: CENTERS OF ACTION AND THE BEAUFORT HIGH

The Arctic Ocean and sea-ice circulation is controlled largely by surface winds associated with prevailing low- and high-atmospheric-pressure fields. The climatological Arctic mean sea-level-pressure field for the Arctic delineates the following main centers of action: In the vicinity of Iceland and southern Greenland, the semipermanent Icelandic Low is characterized by intense



cyclone activity (e.g., Serreze et al. 1997, Moore et al. 2018) (**Figure 2**). In the Pacific sector near the Aleutian Islands is the Aleutian Low, also a confluence of intense cyclone activity (e.g., Overland et al. 1999). The Siberian High, located over northeastern Eurasia, is a seasonal high associated with cold air that is constrained by topography. Lastly, the Beaufort High (BH), centered north of North America, appears as a closed anticyclone in the long-term annual mean (Serreze & Barry 2014). The surface wind field associated with the BH drives the circulation of the BG.

2.1. Seasonality of the Beaufort High

The seasonal cycle of the BH is as follows. From December to February, the Siberian High expands to eliminate the locally closed isobars evident in the mean BH (**Figure 2**). A closed BH becomes apparent in March–May, when the Siberian High weakens due to increased solar heating in spring and a loss of snow over Eurasia (Serreze & Barrett 2011). In summer, the BH and other main pressure centers become weaker and ill defined. These seasonal transitions have been known for some time, described as a prominent BH in winter and a weaker, contracted BH (accompanied by expanded cyclonic circulation in the Eurasian sector) in summer (Gudkovich 1961, Sokolov 1966, Rigor et al. 2002). In the next section, we describe how similar configurations are identified with respect to changes on timescales that are longer than seasonal (Rigor et al. 2002).

2.2. Interannual and Longer-Term Variability of the Beaufort High

There are two main modes of atmospheric circulation in the Arctic, distinguishable by the relative strengths and sizes of the anticyclonic circulation centered over the Canadian sector (i.e., the BH) and the cyclonic circulation centered over the Eurasian sector (an extension of the Icelandic Low) (see Gudkovich 1961, Proshutinsky & Johnson 1997). One mode (here termed mode A) has a prominent BH and a contracted cyclonic circulation, with a Transpolar Drift aligned from the Laptev and East Siberian Seas to Greenland. The other mode (mode B) has a contracted BH and an expanded cyclonic circulation, with the Transpolar Drift axis shifted toward North America (see figure 4 in Proshutinsky & Johnson 1997). These circulation patterns and shifts have been characterized according to the phase of the Arctic Oscillation index (Thompson & Wallace 1998). The high-index phase approximately corresponds to mode B described above, while a low-index phase corresponds to mode A, alternating on timescales of a few years to decades (Rigor et al. 2002).

Variations on timescales even longer than decadal have also been documented in the BH. Kenigson & Timmermans (2021) showed, for example, that there has been a transition from a stronger BH during 1948–1988 to a weaker BH during 1989–2019, commensurate with a shift from weaker to stronger cyclone activity in the Arctic Ocean and Nordic Seas. Zhang et al. (2019) deduced that a BH weakening since the late 1980s can be linked to ozone depletion in the Northern Hemisphere. In particular, they suggested that zonally asymmetric ozone loss leads to a positional shift of the stratospheric polar vortex, which enhances cyclone activity in the Eurasian Arctic troposphere; this increased cyclone activity weakens the BH.

Atmospheric forcing is modulated by the presence of sea ice. Translating the broad patterns of atmospheric pressure and associated surface winds to ocean surface stresses essential for driving the BG first requires a description of the sea ice.

3. SEA ICE: SHAPING A POLAR WIND-DRIVEN GYRE

The presence of sea ice for most of the year in the BG region relates to all aspects of BG water properties, dynamics, and climate.



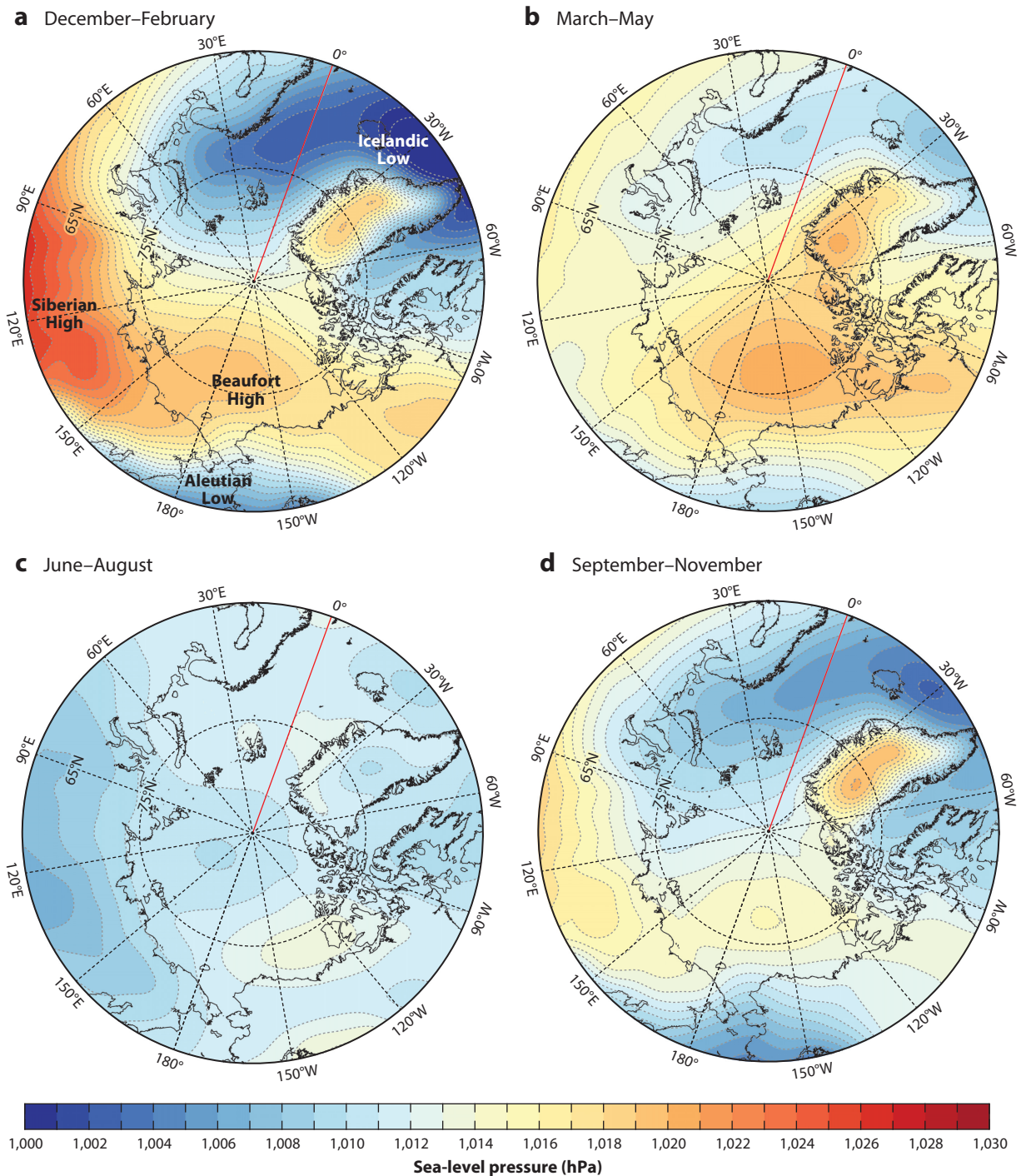


Figure 2

Maps of sea-level pressure indicating the positions of the Icelandic Low, Aleutian Low, Siberian High, and Beaufort High. The maps highlight monthly variability, showing the average sea-level-pressure fields over 1948–2021 for (a) December–February, (b) March–May, (c) June–August, and (d) September–November.



3.1. Seasonal Cycles and Declining Sea-Ice Cover

Seasonally, the Arctic sea-ice extent reaches a minimum every September (approximately 3.92 million km² in 2020) and attains a maximum every March (approximately 14.79 million km² in 2020) (Meier et al. 2021c). The seasonal cycle of sea-ice thickness has been estimated in the BG from sea-ice draft measurements from 2003 to 2012; these measurements indicate that the mean sea-ice thicknesses in May (when sea ice is thickest) are approximately 2 m, and the mean minima are approximately 0.5 m or less in September, when the sea ice is thinnest (Krishfield et al. 2014).

The sea-ice extent has been declining over recent decades, with the losses in sea-ice area most prominent in the summer and fall; the total extent in recent Septembers is approximately 2.3 million km² smaller than in September 1979 (the start of the satellite record). The median September ice edge (15% concentration) during 1981–2010 may be compared, for example, with more recent September sea-ice extents (**Figure 3a**).

A sea-ice thickness decline has also been inferred from satellite data (although not as well as for sea-ice extent), with winter (summer) typical values decreasing from approximately 3.6 m (2.7 m) in the early 1980s to approximately 1.9 m (1 m) in 2008 (Kwok & Rothrock 2009). Mean

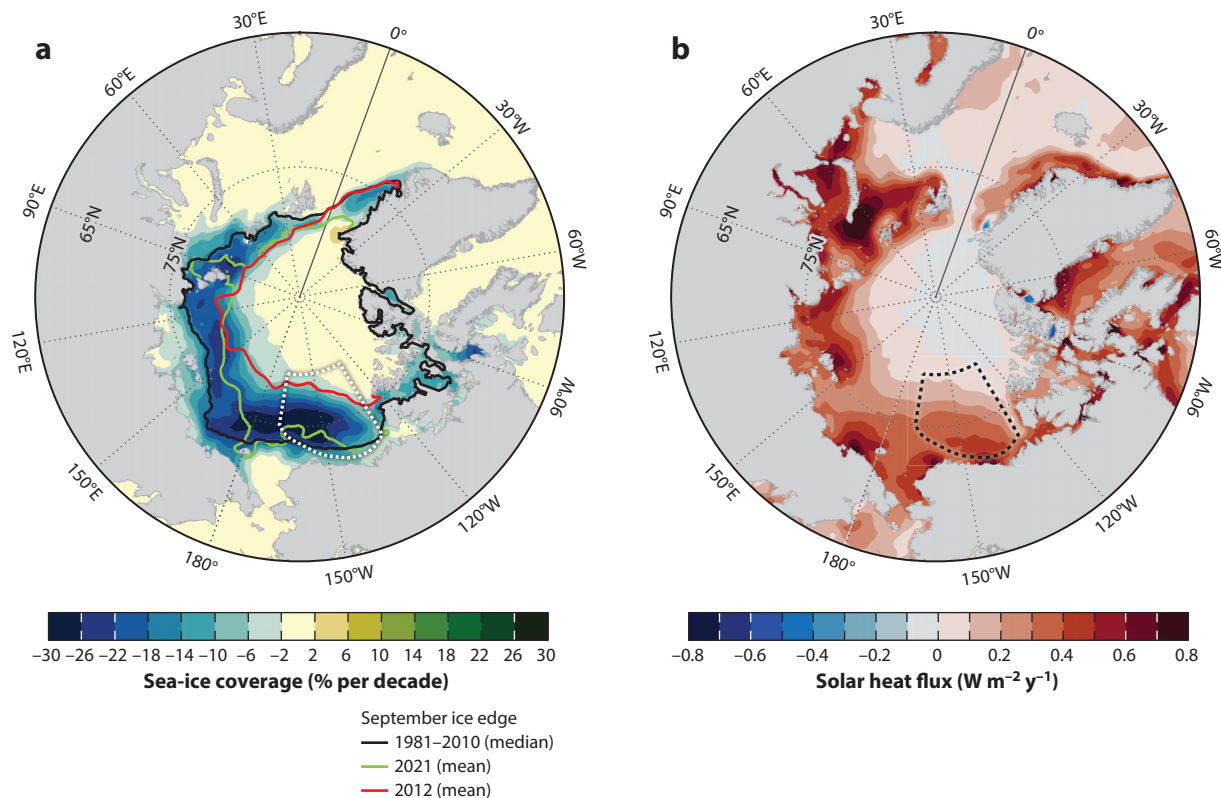


Figure 3

(a) Linear trend in September sea-ice concentration for 1979–2021 in areal percentage of sea-ice coverage per decade. The black contour shows the median September ice edge (15% ice concentration) during 1981–2010, the green contour shows the mean ice-edge position in September 2021, and the red contour shows the mean ice-edge position in September 2012 (the smallest extent on record). (b) Linear trend over 1979–2021 in the flux of solar heat to the ocean, computed as a function of the downward solar irradiance (F), the sea-ice concentration (SIC), and the ocean albedo ($a \approx 0.07$) as $F(1 - a)(1 - SIC)$ (see Perovich et al. 2007). This neglects solar penetration through thin ice.

winter thicknesses in the central Arctic Ocean in 2020–2021 were estimated to be approximately 2 m (Meier et al. 2021c). Sea-ice areal extent and thickness reductions amount to considerable volume losses; in recent summers, for example, total sea-ice volume has been approximately 4,000 km³, which is approximately half the volume of the 1979–2020 average (updated time series from Schweiger et al. 2011).

3.2. Sea-Ice Losses and Surface-Ocean Heating

As sea-ice melts, it exposes the less reflective ocean surface, allowing for increased solar absorption, which drives further ice melt—a cycle known as ice-albedo feedback (Perovich & Richter-Menge 2009). Since 1979, marked sea-ice losses and heat gains by the surface ocean have been observed in every marginal sea of the Arctic basin (**Figure 3**). The most prominent sea-ice losses (in both extent and thickness) have occurred in the BG region (Serreze & Meier 2019, Meier et al. 2021c) (**Figure 3a**). Consequently, the region has seen substantial increases in the amount of solar heating of the upper ocean (Perovich et al. 2007); linear trends over 1979–2021 in the flux of solar heat to the ocean are in the range of 2–5 W m⁻² per decade (**Figure 3b**), which may be compared with typical annual mean solar input fluxes of 10–20 W m⁻² in the region. Averaging over 1981–2010 (often taken as a standard climatological mean period; see **Figure 3a**) shows that the BG region experienced an annual mean solar input of approximately 325 MJ m⁻². In the last decade of the record (2012–2021), the annual mean input was approximately 458 MJ m⁻². For context, the difference between these two time periods (133 MJ m⁻²) equates to approximately 0.6 m of sea-ice thickness melt (taking the latent heat of melting to be 2.67×10^5 J kg⁻¹ and the density of sea ice to be 900 kg m⁻³), demonstrating the importance of the ice-albedo feedback effect in the BG region.

3.3. Influence of the Freeze/Melt Cycle on the Ocean

During the sea-ice growth season (approximately October–May) the BG can be supplied laterally with brine-enriched waters that are produced in the Chukchi shelf regions when open water is continuously exposed while atmospheric temperatures are below freezing (Weingartner et al. 1998, Winsor & Björk 2000). A region of sustained open water (a polynya) is known to form in winter on the northeast Chukchi shelf (Weingartner et al. 2017), where ice grows rapidly and then is continually advected out of the region by winds or melted by warm Atlantic Water that was upwelled onto the shelf [Pisareva et al. (2019) showed that ice advection by wind is the dominant factor]; this process sets up conditions for sustained formation of cold, salty (brine-enriched) waters, salinifying the waters of Pacific Ocean origin on their transit to the BG. In this polynya, sea-ice production can be in the range 9–15 m y⁻¹ (compared with typical ice growth in Arctic shelf regions of approximately 1.5 m y⁻¹), giving rise to an increase in the salinity of the winter waters of up to 2 g kg⁻¹ (Winsor & Chapman 2002). A detailed overview of dense water formed in this region of the Chukchi Sea is given by Williams et al. (2014).

During the melt season (approximately June–September), fresh melt water is returned to the surface ocean. In the Arctic Ocean as a whole, this input of freshwater does not balance ocean salinification in the growth season; each year, approximately 14% of the total sea-ice volume is exported out of the Arctic (see Spreen et al. 2020). In the BG region, Krishfield et al. (2014) showed that before 2006, sea-ice growth led to a local net salinification, with export of sea ice from the region removing freshwater, whereas after 2006, the region experienced net freshening as a result of local sea-ice melt dominating. An ocean and sea-ice state estimate model study corroborated this general shift to the greater influence of local sea-ice melt (Fukumori et al. 2021).



3.4. Sea-Ice Modulation of Wind Momentum Transfer

Sea ice, which is constantly in motion driven by wind forcing and surface-ocean currents, generally follows a large-scale clockwise circulation in the BG (**Figure 4**). Typical ice-drift speeds range from a few to $O(10)$ centimeters per second, while typical surface winds in the region are several meters per second. The presence of sea ice in low concentrations can increase the transfer of wind momentum into the ocean (because ice-ocean drag is greater than air-ocean drag), while higher sea-ice concentrations can suppress momentum transfer when internal ice forces inhibit pack motion (Martin et al. 2014, Cole et al. 2017). This general behavior has a strong dependence on sea-ice morphology (e.g., Brenner et al. 2021).

Inferences from hydrography and remote sensing (e.g., Armitage et al. 2016, 2017) indicate a year-round surface-ocean geostrophic flow on the order of several centimeters per second (**Figure 4e,f**). We use these estimates together with winds and sea-ice concentration/motion to compute the Ekman pumping that spins the BG up or down. Following the methods outlined by Meneghello et al. (2018), one can calculate the Ekman vertical velocities for 2003–2021 from surface-ocean stresses that are a combination of ice-ocean and air-ocean stresses. The available record of geostrophic currents computed from dynamic ocean topography spans only 2003–2014 (Armitage et al. 2016, 2017); for calculations after 2014, we use the 2014 values of geostrophic currents under the assumption that variability in these flows is small and does not significantly affect the overall results. While it is essential to take geostrophic currents into account, variations in Ekman vertical velocities are influenced primarily by changes in the strength of the wind-stress curl and sea-ice concentration (e.g., Meneghello et al. 2018).

In summer, there is broad, strong downwelling in the central BG forced by anticyclonic winds acting directly on the surface ocean and the motion of sea ice in low concentrations (**Figures 4c** and **5a**). Each winter, sea-ice concentrations increase and the sea-ice pack becomes less mobile in response to wind forcing (i.e., internal ice stresses dissipate wind input). At the same time, the BG ocean geostrophic flow remains. Consequently, friction at the ice-ocean interface drives broad Ekman upwelling in this season that slows the BG (Proshutinsky et al. 2002, Dewey et al. 2018, Meneghello et al. 2018) (**Figure 5b**). In this way, the seasonal expansion of sea-ice cover in the region acts as a dissipative source of wind-energy input, stabilizing the BG such that it does not spin up indefinitely.

It is notable that downwelling appears to be much stronger in September even though September is generally characterized by weaker anticyclonic wind-stress curl. This is because there is a stronger cyclonic surface stress in March, due to the influence of anticyclonic geostrophic surface currents under the relatively immobile sea ice, than in September, when the sea-ice concentration is at its seasonal minimum. On average, downwelling is typically strongest in September and October, while the months of January–March are characterized by areal-mean Ekman upwelling over the region (see figure 3 in Meneghello et al. 2018).

4. WATER MASSES OF THE BEAUFORT GYRE: SOURCES, STRUCTURE, AND CIRCULATION

The freshwater that maintains the strong halocline stratification is supplied to the BG by three main sources: sea ice (Section 3), meteoric water, and Pacific Water. We describe the latter two next.

4.1. Meteoric Water Supply

The difference between precipitation and evaporation over the Arctic Ocean contributes a net flux of approximately $2,000 \text{ km}^3 \text{ y}^{-1}$ to the ocean (Jakobson & Vihma 2010, Vihma et al. 2016).



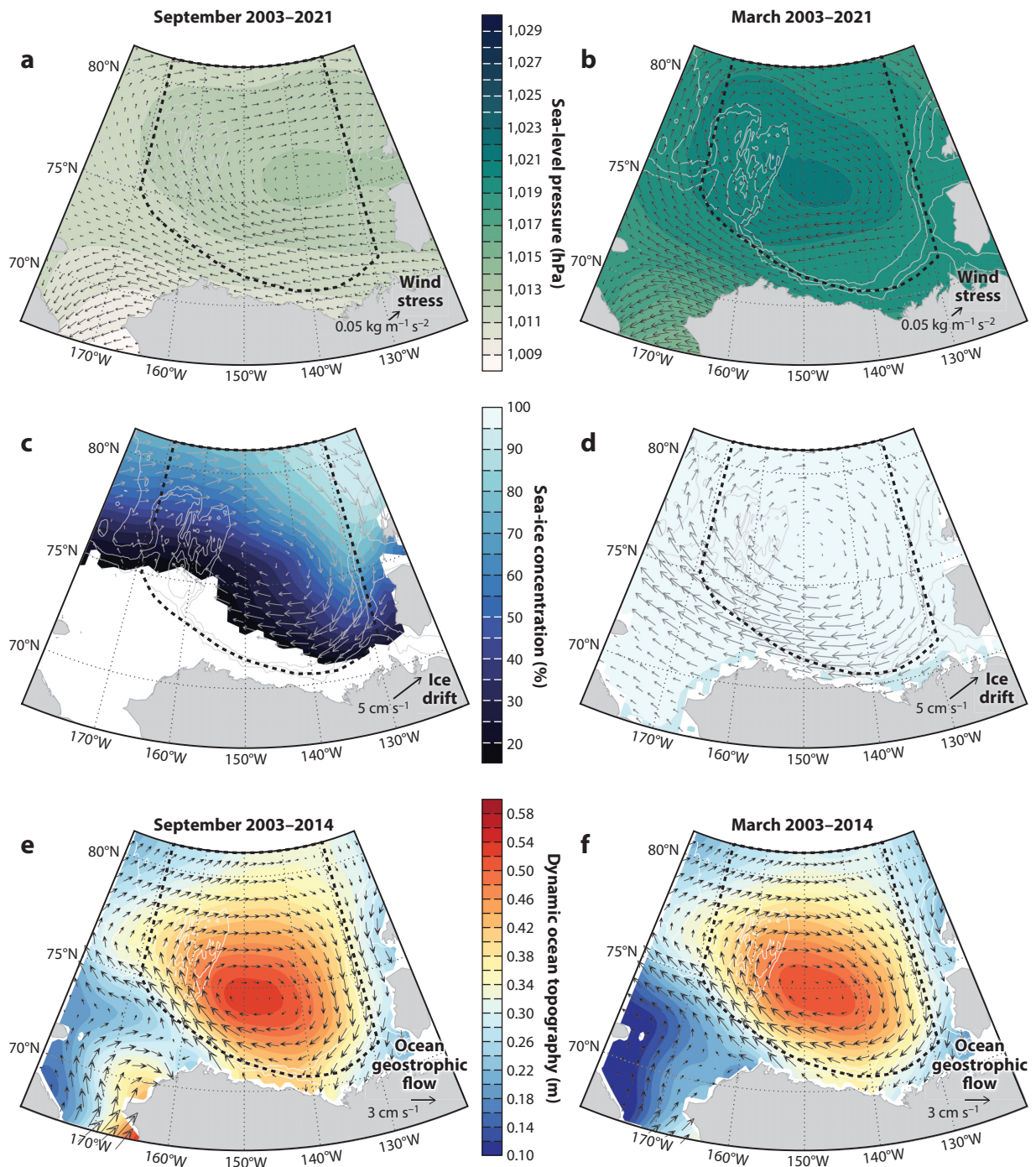


Figure 4

Mean forcing and flow fields in the Beaufort Gyre region for (left column) September 2003–2021 and (right column) March 2003–2021. (a,b) Sea-level pressure (colors) and wind stress (arrows). (c,d) Sea-ice concentration (colors) and ice-drift speed (arrows). (e,f) Dynamic ocean topography (colors) and ocean geostrophic flow (arrows). Note that panels e and f are only for 2003–2014 because the available record of geostrophic currents covers only that period.



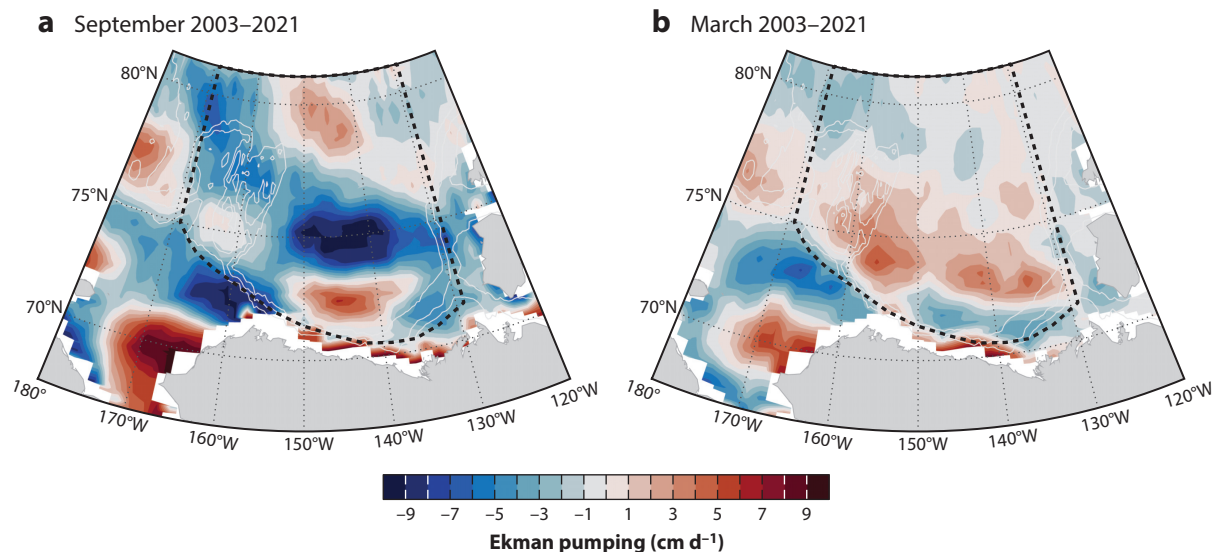


Figure 5

Mean vertical Ekman pumping for (a) September and (b) March over 2003–2021. When sea-ice concentrations are low (**Figure 4c**), winds drive downwelling (blue) over most of the Beaufort Gyre region, while when sea ice is extensive (**Figure 4d**), friction between the geostrophic flow and sea ice gives an upwelling (red) contribution.

In addition, net precipitation over land north of 50°N feeds rivers that drain into the Arctic Ocean, supplying approximately $4,000 \text{ km}^3 \text{ y}^{-1}$ (see Haine et al. 2015). The circulation pathways for the river waters entering the BG relate to the configuration of the large-scale wind-driven ocean circulation (e.g., Timmermans et al. 2011, Morison et al. 2012, Proshutinsky et al. 2019). The Mackenzie River (**Figure 1b**), which has an annual discharge of approximately $300 \text{ km}^3 \text{ y}^{-1}$ (Holmes et al. 2019), is believed to be the main contributor of riverine water to the BG over the period 2003–2018 (Proshutinsky et al. 2019).

4.2. Pacific Water Source

The presence of waters with origins in the Pacific Ocean is a major distinguishing characteristic of the BG water column. The northward flux of Pacific Water through the approximately 85-km-wide, 50-m-deep Bering Strait is approximately 1 Sv ($10^6 \text{ m}^3 \text{ s}^{-1}$) (e.g., Coachman & Aagaard 1966, Aagaard et al. 1985). There is a significant annual cycle in this transport, with values ranging from approximately 0.4 Sv in winter to 1.3 Sv in summer (Woodgate et al. 2005). The mean northward current, typically several tens of centimeters per second in strength, is driven by both winds and pressure forcing (a pressure head) associated with a north–south slope in the sea-surface height (lower in the north) (Coachman & Aagaard 1966).

Woodgate & Peralta-Ferriz (2021) found that the northward transport via the Bering Strait increased by approximately 0.1 Sv per decade in the period 1990–2019. The amount of heat entering (relative to -1.9°C) has also increased to approximately $6 \times 10^{20} \text{ J y}^{-1}$ in 2017–2018, compared with approximately $3 \times 10^{20} \text{ J y}^{-1}$ in the 1990s; the most recent years of the record indicate October/November ocean temperatures up to 6°C , at least several degrees warmer than those in the early part of the record. This excess heat is responsible for sea-ice melt and, in turn, enhanced solar warming of the surface ocean (Woodgate et al. 2010). Notably, Woodgate & Peralta-Ferriz (2021) also found that waters fluxing through the strait in winter (Pacific Winter Waters) have

freshened significantly over the duration of the record, from values typically saltier than 32.7 in the 1990s to values fresher than 32.3 since 2015, which they suggested has implications for the ventilation of the BG halocline.

In winter, waters over the Chukchi shelf are vertically homogenized by cooling, brine rejection during ice formation, and wind mixing. Spall (2007) showed that for temperature, the Bering Strait influence on the water properties of the Chukchi shelf is limited largely to the southern region near the strait, local air–sea exchange being increasingly important moving north. This finding was echoed by Steele et al. (2010), whose seasonal heat budget analysis for waters in the Chukchi–Beaufort region highlighted the importance of local exchange across the air–sea interface.

The outflow from Barrow Canyon (off the northwest coast of Alaska, feeding from the Chukchi Sea to the Beaufort Sea) is a key site for delivery of Pacific Water to the shelf break, supplying shelf-slope currents to the east along the Beaufort shelf break or to the west along the Chukchi slope, depending on the direction of the local winds (Corlett & Pickart 2017, Boury et al. 2020). Ultimately, waters at the margins of the Chukchi Sea ventilate the entire BG halocline over the deep Canada Basin (we refer to this as the interior BG, in contrast to its margins). For example, Lin et al. (2021) showed that Pacific Water originating at Barrow Canyon is transported westward before leaving the surface north of the Chukchi slope and being transported into the interior BG. There exists a region of strong time-mean Ekman downwelling in the southwest BG/Chukchi shelf region (approximately 73°N, 165°W; **Figure 5**), with downwelling rates (approximately 6 cm d⁻¹) that correspond to a vertical transport of approximately 0.05 Sv (Timmermans et al. 2017, Meneghello et al. 2018). Furthermore, a surface front exists at the southwest boundary of the BG between surface waters that are relatively warm (in summer and fall) and salty to the south and the relatively cool and fresh surface BG waters to the north; the position of the front is approximately along the 300-m isobath (i.e., the southwest boundary of the BG region). The south side of the front is characterized by a deeper mixed layer; water on this side can be subducted (by vertical Ekman pumping plus lateral induction) below the mixed layer on the north side (see Timmermans et al. 2017). Processes that factor in this subduction may include surface buoyancy forcing, the configuration of local winds, fluid instabilities, and eddy fluxes (e.g., Spall et al. 2008, Gong & Pickart 2015, Lin et al. 2021).

Seasonally, warm waters are subducted under the BG mixed layer in summer, and waters at freezing temperature are subducted in winter, with the relatively fresher summer waters effectively being isolated by stratification from being pushed out by cold winter waters (Timmermans et al. 2017). Once the Pacific Water has left the surface, it is likely transported laterally into the interior by the anticyclonic BG flow along a broad helical pathway to occupy the BG halocline (Timmermans et al. 2014).

4.3. Beaufort Gyre Water-Column Structure

Sources of freshwater and heat and dynamical wind forcing set up the BG water-column structure, which we review here with representative water-column profiles (**Figure 6**). The freshest waters are found in the surface mixed layer, typically around the local freezing temperature, which ranges from a few meters deep in summer up to approximately 40 m deep in winter (Toole et al. 2010, Peralta-Ferriz & Woodgate 2015). Cole & Stadler (2019) found that BG winter mixed layers generally deepened by approximately 9 m over 2006–2017. The change was accompanied by winter mixed-layer salinity increases (approximately 1 g kg⁻¹) and weakened stratification across the mixed-layer base, which were attributed predominantly to reduced surface freshwater input rather than increases in vertical mixing. Peralta-Ferriz & Woodgate (2015) pointed out that in the BG region, seasonal sea-ice melt cannot explain the seasonal cycle in mixed-layer salinity, and



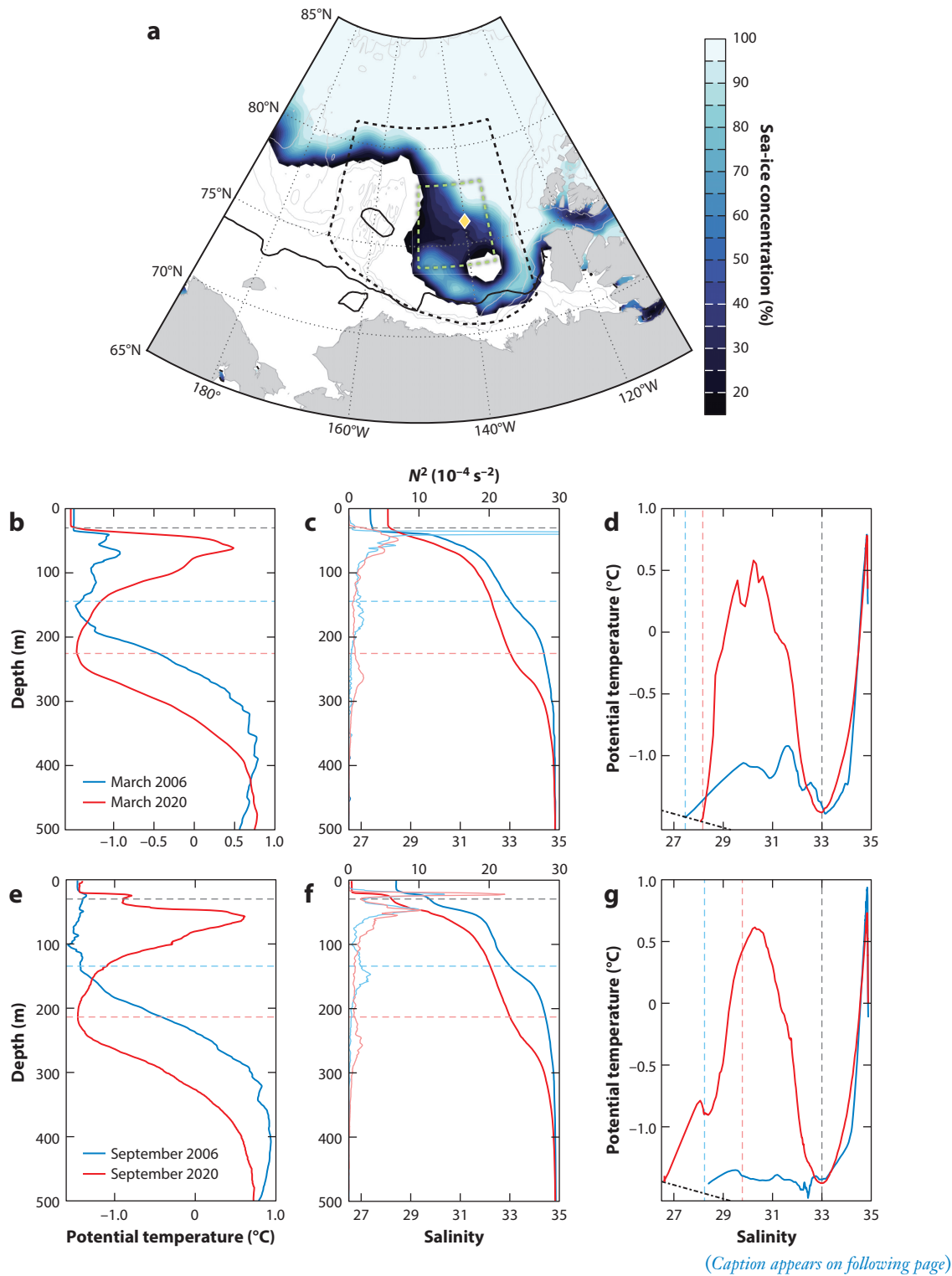


Figure 6 (Figure appears on preceding page)

(a) Map of the Beaufort Gyre region showing the September 2020 sea-ice concentration (colors) and September 2006 sea-ice edge (black contour). The dotted green line delineates the central Beaufort Gyre, and the yellow diamond shows the location of the profiles in panels b–g. (b–d) Profiles from March (2006, blue; 2020, red) of potential temperature (panel b); salinity versus depth, with lighter lines (top x axis) showing the buoyancy frequency; and potential temperature versus salinity (panel d). (e–g) The same as panels b–d but for September. In panels b, c, e, and f, the horizontal dashed lines indicate 30-m depth (gray) and the depths of $S = 33$ (colored red or blue by profile). In panels d and g, the dot-dashed black lines indicate the freezing temperature at zero pressure, and vertical dashed lines mark $S = 33$ (gray) and the salinity values at 30-m depth (colored red or blue by profile).

they referred to the importance of river and Pacific Water sources in setting mixed-layer properties. Below the base of the mixed layer, a near-surface temperature maximum layer is often a feature formed during the summer melt period (Maykut & McPhee 1995, Jackson et al. 2010, Timmermans 2015); a thin near-surface temperature maximum layer is visible in **Figure 6e,g**.

The most distinctive feature of the BG water column is the warm Pacific Summer Water (PSW) layer between approximately 30- and 200-m depth (**Figure 6**). As suggested by the differences between 2006 and 2020 profiles (**Figure 6**), PSW has exhibited prominent warming in recent decades, which we quantify in Section 6. Below the PSW layer in the BG halocline sits a saltier, cooler (close to freezing temperature) layer, the Pacific Winter Water layer. Pacific Waters are often delineated by their salinities, with PSW generally being in the salinity range of 29–33 (Timmermans et al. 2014) and Pacific Winter Water centered around a salinity of 33.1 (Shimada et al. 2005).

The Pacific Waters set up a complex stratification that has implications for the dynamics and distribution of energy in the BG water column. The strongest buoyancy stratification (**Figure 6c,f**) is at the base of the mixed layer, with a secondary peak in stratification in September profiles that is associated with the summer halocline. At greater depths (between 150 m and 250 m in the profiles shown in **Figure 6**), yet another peak in stratification is found at the base of the Pacific Winter Water layer. The weakly stratified Pacific Winter Water layer is a pycnostad; this layer originates at the surface in the Chukchi shelf regions, where winter mixing homogenizes the full water column. Intra-halocline eddies are prevalent in the BG at depths between the two buoyancy stratification peaks, where water-column kinetic energy is concentrated (Zhao et al. 2016, 2018). The variety of BG halocline eddies is consistent with both quasi-geostrophic adjustment to a potential vorticity anomaly in this stratification (Zhao & Timmermans 2015) and results of linear stability analysis based on this stratification structure (Meneghello et al. 2021).

Water of Atlantic Ocean origin sits below the Pacific Waters in the BG, with a maximum core temperature at approximately 400-m depth (**Figure 6**). This Atlantic Water exhibits an assemblage of sublayers at its top boundary associated with a double-diffusive staircase (Padman & Dillon 1987) and centered on its core, associated with thermohaline intrusions (Carmack et al. 1998). A discussion of the Atlantic Water is beyond the scope of this review; readers may refer to, for example, works by Karcher et al. (2007), who examined the circulation of the Atlantic Water layer as it relates to the circulation of upper BG waters, and Grabon et al. (2021), who explored the ocean state over the period 2004–2017. We focus our attention here on the circulation of surface and Pacific Water layers, as they exhibit the most prominent changes with respect to freshwater and heat content.

4.4. Circulation

Hydrographic measurements in the BG reveal the broad bowl structure of isopycnal (or, equivalently, isohaline) surfaces associated with a surface-intensified anticyclonic gyre. The spatial distribution of the $S = 33$ practical salinity surface is shallowest at the margins of the BG region



and up to 100 m deeper in the interior (central BG) (**Figure 7**). Representative north–south sections through the BG along 140°W show this structure in depth and also indicate how the highest heat content in the PSW layer is found in the central BG on this meridian (**Figure 7**). Corresponding sections along 150°W show a similar structure. Notably, between the early years and the later years shown, there is an appreciable deepening of isopycnals manifesting the BG spin-up during this time, and a significant warming of PSW.

Dynamic heights computed from hydrographic measurements spanning 2008–2011 indicate surface geostrophic currents as high as 10–15 cm s⁻¹ at the southern periphery of the BG (see figure 1a in McPhee 2013). Direct velocity measurements indicate that the vertical structure of the flow field decays with depth such that mean current speeds are only approximately 1 cm s⁻¹ below approximately 300 m, although the record is dominated by energetic mesoscale eddies with horizontal speeds that can be several tens of centimeters per second (Zhao et al. 2018). Satellite dynamic ocean topography fields reveal a notable change on the western flank of the BG, where surface currents (to the northwest; **Figure 4e,f**) were generally approximately 2–4 cm s⁻¹ before 2007 and then increased to speeds of approximately 5–8 cm s⁻¹ for the remainder of the record (through 2014). Also notable in these fields is that the center of the BG circulation shifted northward by a few hundred kilometers over 2003–2014, which was inferred to be related to the strength and position of the BH (Armitage et al. 2017, Regan et al. 2019).

5. THE BEAUFORT GYRE FRESHWATER RESERVOIR

The BG has long been known as the largest freshwater reservoir of the Arctic Ocean (Aagaard & Carmack 1989). Freshwater maintains the strong halocline stratification of the BG, which is important to ocean heat, momentum and nutrient fluxes, and circulation. Ocean freshwater content is commonly defined relative to a reference salinity and is computed as a depth integral of relative freshwater from the surface ocean to the depth of the reference salinity. [Schauer & Losch (2019) criticized this framework, preferring to work with the full salinity estimates.] The choice of reference salinity is generally taken to be 34.8 (following Aagaard & Carmack 1989), the approximate value of the Arctic Ocean's mean salinity; the 34.8 isohaline is at approximately 400-m depth in the BG (see Carmack et al. 2016). Haine et al. (2015) estimated the 2000–2010 average total Arctic Ocean freshwater volume to be 101,000 km³, with approximately 25% of that stored in the BG.

Ocean freshwater content in the BG region shows significant interannual variability, with periods of both rapid change and relative stability (Proshutinsky et al. 2009, 2019, 2020). Yearly hydrographic sampling under the Beaufort Gyre Observing System/Joint Ocean Ice Study has allowed for a quantification of the year-to-year change in freshwater content since 2003 (Proshutinsky et al. 2009) (**Figure 8**). Overall, freshwater content has been increasing; total freshwater content in 2021 (approximately $22 \pm 3 \times 10^3$ km³) was approximately 5×10^3 km³ greater than it was in 2003.

5.1. Variability and Trends

Seasonal and longer-term changes in BG freshwater may be broadly attributed to atmospheric circulation changes (Proshutinsky et al. 2009). Under sustained anticyclonic forcing, for example, mass is transported laterally in the surface Ekman layer, converging sea ice and low-salinity surface waters and spinning up the gyre. Waters are pumped down into the halocline at the periphery of the BG (where isopycnals outcrop at the surface), inflating the gyre (BG potential vorticity dynamics were described in Timmermans & Marshall 2020).

In the seasonal cycle, freshwater content in the BG region is typically maximal in December and minimal in April, with a difference between these two periods of approximately



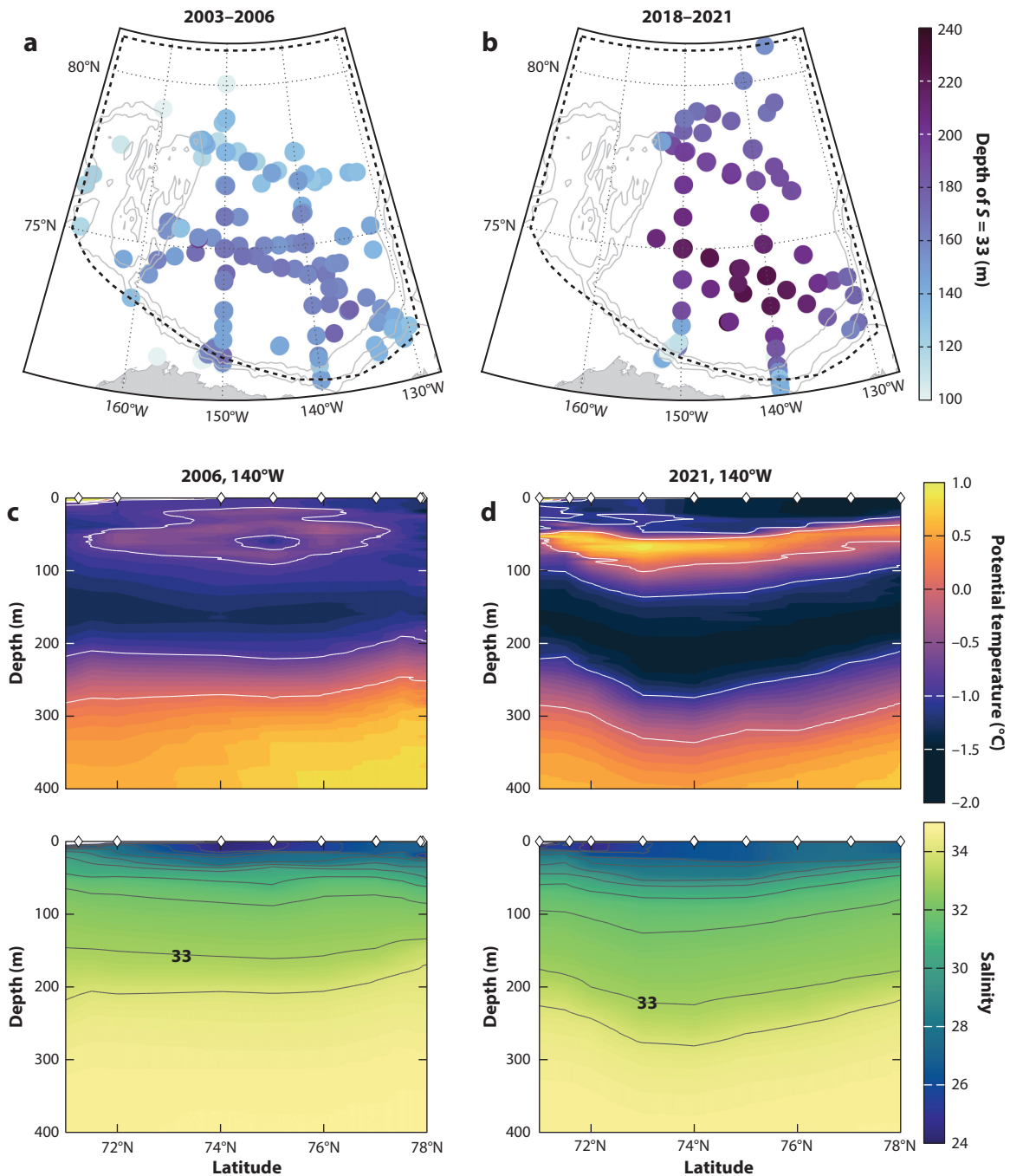


Figure 7

(*a,b*) Maps of the Beaufort Gyre region indicating the depth of the $S = 33$ isohaline for 2003–2006 (panel *a*) and 2018–2021 (panel *b*). (*c,d*) Depth–latitude sections at 140°W of potential temperature (*top*) and salinity (*bottom*) for 2006 (panel *c*) and 2021 (panel *d*). The diamonds at the top indicate station locations.



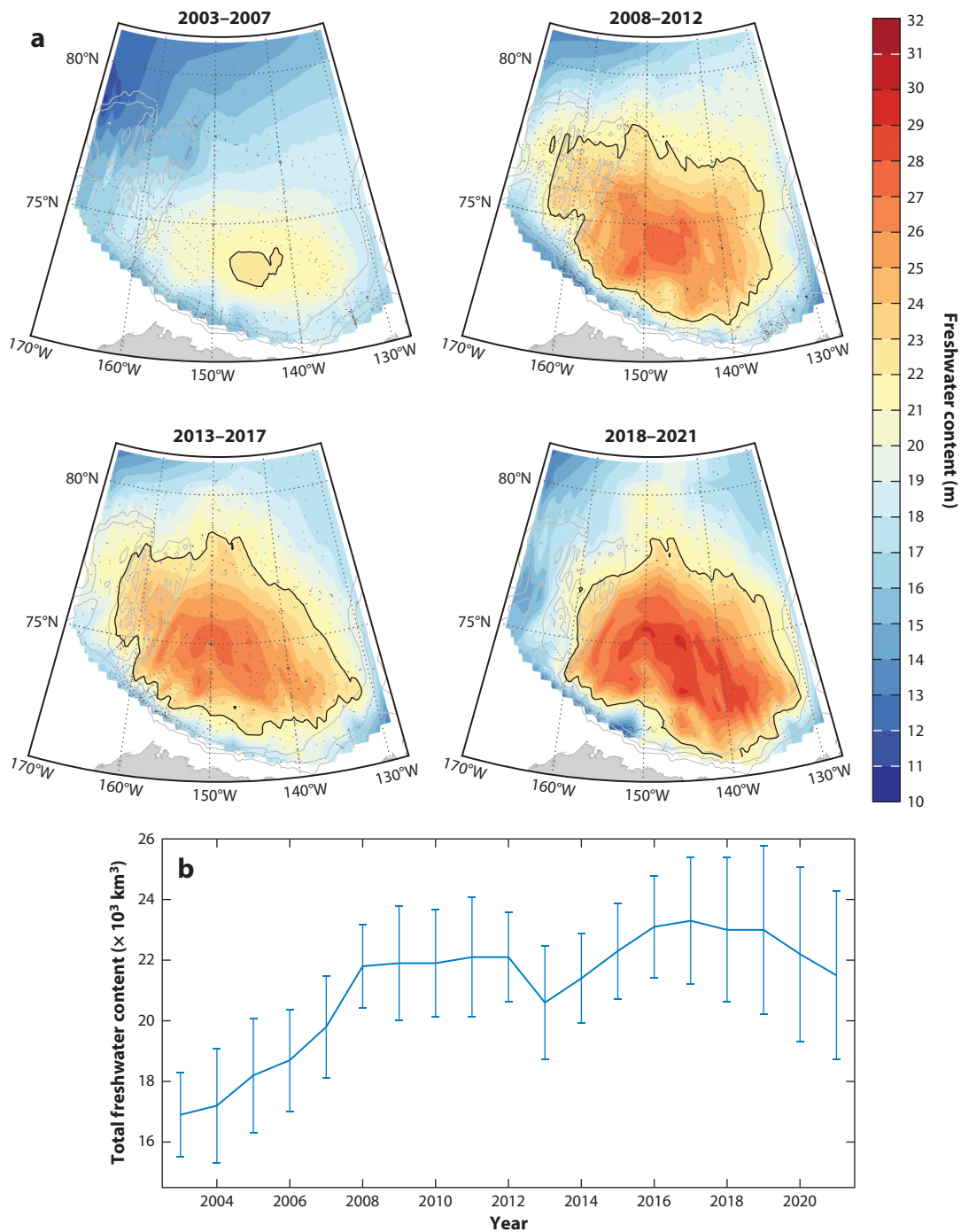


Figure 8

(a) Maps of freshwater content (relative to salinity 34.8) for the years indicated. The black dots show the locations of observations taken sometime from July to October in the respective years, and the black line shows the 22-m freshwater content contour. (b) Time series of total freshwater content and root mean square error in the Beaufort Gyre region. Freshwater calculations were updated from Proshutinsky et al. (2009, 2020).

6.16 Timmermans • Toole



4,000–5,000 km³ (Proshutinsky et al. 2009). For reference to the average freshwater content per unit area (**Figure 8a**), the typical amplitude of the seasonal cycle in the central BG is approximately 2 m. Subtleties emerge on detailed examination of this overall seasonal cycle, with observations indicating two peaks in freshwater content: the annual maximum in winter, when wind-forced Ekman pumping is strongest, and a secondary local peak, dominated by changes in the surface ocean, in June, when freshwater availability from rivers and ice melt is maximal (Proshutinsky et al. 2009, Armitage et al. 2016, Proshutinsky et al. 2019).

The largest increase in BG freshwater content was observed between 2003 and 2008 (**Figure 8b**), driven by anomalous anticyclonic wind forcing and associated wind-stress gradients, which were particularly strong in 2007 (Proshutinsky et al. 2009). Freshwater content remained relatively constant between 2008 and 2012, which may be related to a general weakening of anticyclonic wind-stress curl and to a greater role of upwelling under concentrated sea-ice cover in the winter months (e.g., Meneghello et al. 2018). This is corroborated by moored time series of isopycnal displacements that indicate a shoaling of isopycnals during this time (Proshutinsky et al. 2019). A freshwater flux out of the region in 2012–2013 (giving rise to the local minimum in freshwater content in 2013; **Figure 8b**) is attributed to even further weakening of the anticyclonic wind forcing, such that upwelling resulting from anticyclonic geostrophic currents interacting with the underside of sea ice dominated the (weaker) wind-driven convergence (Proshutinsky et al. 2019).

Understanding BG freshwater accumulation is complicated by the fact that freshwater sources (i.e., anomalies from sea-ice melt, net precipitation, Pacific inflows, and river influxes) vary temporally and spatially. Measurements and modeling analyses suggest that waters derived from sea-ice melt, waters originating in the Bering Strait, and waters from the Mackenzie River were the dominant contributions to BG freshwater over 2003–2018, constituting approximately 41%, 35%, and 15% of the total increase, respectively (see figure 11 in Proshutinsky et al. 2019). Local sea-ice melt contributed less than 10% of the total freshwater accumulation in the BG over that period (Proshutinsky et al. 2019), with the largest contributions after 2007, coinciding with a shift toward thinner ice in the BG (Krishfield et al. 2014). Fukumori et al. (2021) employed an ocean and sea-ice state estimate model to conclude that after 2007, the stronger anticyclonic wind stress intensified the local meltwater contribution via greater convergence of sea ice into the region and its subsequent melt.

Notably, the observed BG freshwater changes are unlikely to be effectively simulated in the climate models that are used in IPCC Assessment Reports. For example, Rosenblum et al. (2021) analyzed model output in the BG region from two versions of the Community Earth System Model (CESM1 and CESM2), comparing model simulations and observations collected during 1975 and 2006–2012. They showed that simulations produce a saltier and more weakly stratified water column than indicated by the observations. Rosenblum et al. (2021) related this inconsistency to excessive ocean mixing in the models, which has significant consequences for projections of sea ice, ocean heat transport, ice-albedo feedback, and primary productivity.

5.2. Stabilization of the Beaufort Gyre

Observations indicate that even under sustained anticyclonic winds, the BG does not increase its circulation and accumulate freshwater indefinitely; rather, under-ice friction in winter can dissipate energy and stabilize the BG, as described in Section 3.4. Stabilization of the BG may additionally involve the dissipation of available potential energy by ocean eddies. Ocean eddies resulting from baroclinic instability of the background flow field are thought to act as a balance on the wind-driven momentum flux into the BG (e.g., Davis et al. 2014, Manucharyan et al. 2016, Dewey et al. 2018, Armitage et al. 2020). In addition to fluxing potential energy downgradient, eddies transport freshwater out of the BG, limiting freshwater accumulation. Velocity measurements analyzed to



quantify eddy diffusivities across the BG reveal that there may be sufficient water-column eddy kinetic energy to balance the winds (Meneghello et al. 2017); the general theory was reviewed by Timmermans & Marshall (2020).

Exploring these balances to understand adjustment timescales (i.e., the response of the BG to a step change in surface forcing) is essential for understanding the accumulation and release of freshwater as surface forcing changes, as well as the influence of past surface forcing in setting BG properties. Considering BG equilibration resulting entirely from the negative feedback between surface-ocean geostrophic currents and ice-ocean stress yields adjustment timescales of approximately 1–2 years. This may be contrasted with timescales on the order of a decade required to equilibrate when eddy diffusivity acts alone (e.g., Davis et al. 2014, Manucharyan et al. 2016). Doddridge et al. (2019) presented an analytical theory for BG stabilization that includes dissipation by both sea ice and mesoscale eddies and a three-way balance among wind stress, ice-ocean stresses, and eddy diffusivity. They showed that, for typical values of eddy diffusivity and ice-drift speeds, adjustment timescales are generally somewhere between the two end members above (a few to 10 years).

5.3. Circulation Regimes

Shifts in the large-scale wind patterns on decadal and longer timescales have been used to explore variations in the wind-driven BG. For example, Morison et al. (1998) documented a shift (which they related to the phase of the Arctic Oscillation), beginning in the early 1990s, to an expansion/intensification of the ocean cyclonic circulation in the Eurasian Basin (this is associated with the mode B atmospheric circulation pattern described in Section 2.2). Morison et al. (2021) suggested that this enhanced cyclonic circulation has persisted for approximately the past three decades, coinciding with a more intense but more confined BG. This is consistent with a generally intensified and expanded Icelandic Low over these decades (Kenigson & Timmermans 2021).

Past studies of decadal BG variability have invoked its capacity to store and release sufficient volumes of freshwater to have consequences that feed back to the atmospheric circulation (Proshutinsky & Johnson 1997; Dukhovskoy et al. 2006a,b; Proshutinsky et al. 2015). Proshutinsky et al. (2015) suggested that a strong BH is conducive to the accumulation of freshwater in the BG and to a reduction in oceanic freshwater (and, therefore, stratification) in the Nordic Seas (i.e., the vicinity of the Icelandic Low) because of commensurate reduced freshwater export from the Arctic. Under this hypothesis, there is an intensification of Nordic Seas cyclone activity because reduced stratification there allows for enhanced deep-ocean convection and ocean-to-atmosphere heat fluxes. In turn, the BH is weakened by this expanded cyclone activity, allowing for a release of freshwater from the BG, enhanced freshwater in the Nordic Seas, and suppressed deep convection and cyclone activity there. The entire cycle can repeat in a decadal oscillation (see Proshutinsky et al. 2015).

6. BEAUFORT GYRE WARMING: INCREASING HEAT CONTENT IN THE HALOCLINE

Accompanying sea-ice losses, increased solar absorption, and increased freshwater in the BG region in recent decades, there has been a dramatic increase in upper-ocean heat content. Since at least the late 1980s, the BG has experienced a significant buildup of heat in its PSW, concentrated in the central BG in a similar pattern to that of freshwater (see figure 2 in Timmermans et al. 2018). Timmermans et al. (2018) showed that this accumulation of heat in the central BG is consistent with the observed warming of the PSW source waters in the northern Chukchi Sea region in recent years (with increased solar absorption into the upper ocean there as a result of sea-ice retreat; see Danielson et al. 2020) (Figure 3).



To quantify this change in the PSW layer while avoiding spatial variability influencing the time series, we consider an intensively sampled region of the central BG (shown in **Figure 6a**). To minimize the influence of the seasonally varying surface waters (in approximately the upper 30 m) and potential for aliasing, we calculate the heat content (relative to the freezing temperature) in the layer between 30 m and the depth of the $S = 33$ isohaline (see **Figure 6b–g**). Over the period 2004–2021, the heat content of the PSW layer in the central BG has approximately doubled (**Figure 9**). Contributions to heat content from either the change in layer-averaged temperature or the change in layer thickness can have varying influences from year to year, but neither dominates the overall heat content trend (Timmermans et al. 2018). Before the 2000s, typical values of heat content per unit area in the central BG PSW layer were approximately $2 \times 10^8 \text{ J m}^{-2}$ (Timmermans et al. 2018). In the most recent years (2019–2021), central BG estimates of heat content per unit area reach $8 \times 10^8 \text{ J m}^{-2}$ at some locations (**Figure 9f**). Notably, the additional heat is enough to melt approximately 1 m of sea ice, although this would require that it be made available to the surface waters in direct contact with the sea ice. (We further examined the heat content in the layer bounded by $S = 33$ and $S = 34.86$, a span that defines the layer below the PSW, encompassing the Atlantic Water core. There is no significant increasing or decreasing trend in heat content, thickness, or layer-averaged temperature in this layer over the period 2004–2021.)

The heat content between 10-m and 30-m depth (see **Figure 9g**) exhibits only seasonal variability over the course of the record. The central BG Pacific Waters do not tend to exhibit variability on seasonal timescales (e.g., compare March and September 2020 profiles in **Figure 6b**) because they are too deep to be influenced by local solar radiation and the strong halocline stratification inhibits vertical heat fluxes from the warm PSW layer (Toole et al. 2010).

While strong stratification and weak mechanical mixing at the base of the surface layer inhibit vertical heat fluxes to the underside of sea ice, there is at least a small fraction of heat lost from the warm layer by vertical diffusion. Given turbulent diffusivities at the base of the BG mixed layer in the range of approximately 10^{-7} – $10^{-6} \text{ m}^2 \text{ s}^{-1}$ (Shaw & Stanton 2014), we estimate vertical heat fluxes into the mixed layer in the range 0.02–0.8 W m^{-2} . For context, an excess of 1 W m^{-2} (equivalent to a sea-ice thickness reduction of approximately 0.1 m y^{-1}) in the Arctic energy budget is sufficient to account for the observed thinning of Arctic sea ice in recent decades (see, e.g., Kwok & Morison 2011). At the high end of these flux values, the PSW layer would lose up to half of its heat content in approximately a decade by vertical diffusive fluxes alone (for the mean value of PSW heat content in **Figure 9g**). Dosser et al. (2021) deduced an increase in BG halocline turbulent diffusivities from values of $(3 \pm 1) \times 10^{-7} \text{ m}^2 \text{ s}^{-1}$ in the 2004–2010 period to $(7 \pm 1) \times 10^{-7} \text{ m}^2 \text{ s}^{-1}$ in the 2011–2019 period, resulting from an increase in internal-wave-driven turbulent kinetic energy dissipation rate. They showed that between these two time periods, heat fluxes across the halocline increased by an order of magnitude (from 0.02 W m^{-2} to 0.21 W m^{-2}) both because of these larger turbulent diffusivities and because of temperature gradients that were larger by a factor of three.

7. FUTURE QUESTIONS

Extensive observations of the BG system in recent decades have documented pronounced sea-ice losses, increased freshwater, and a sizable buildup of ocean heat. There are many open questions surrounding the future trajectories and implications of these changes.

We have seen how the existence of a concentrated sea-ice cover plays a role in stabilizing the BG and seasonally regulating freshwater convergence. Under continued sea-ice losses (including an impending milestone in the shift to a seasonally ice-free Arctic), will sea ice continue to play this role, or will eddy fluxes be the sole balance for the wind driving? Under a likely scenario



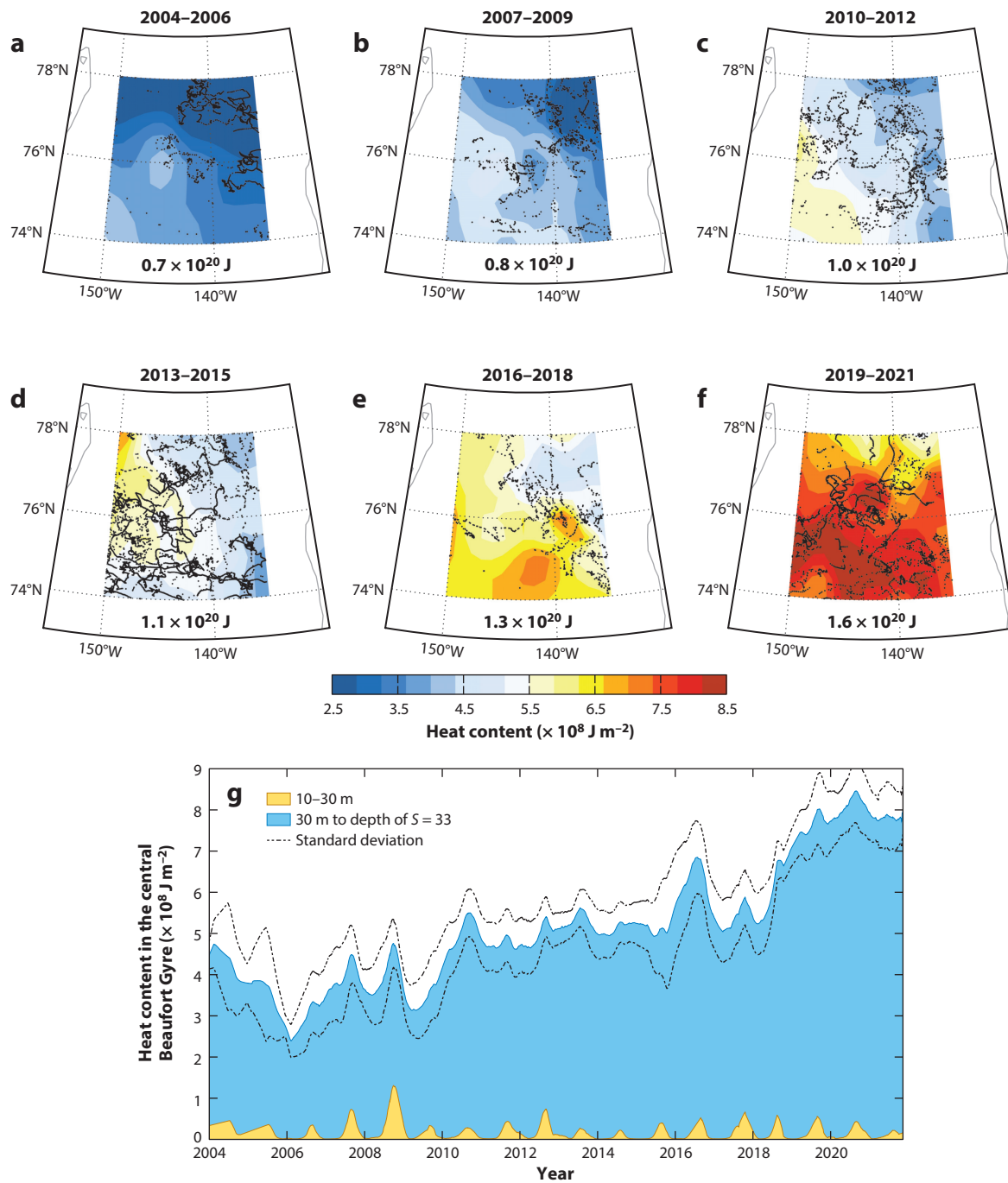


Figure 9

(a–f) Maps of heat content relative to the freezing temperature integrated between 30-m depth and the depth of $S = 33$ for all profiles (black dots) over all seasons in the central Beaufort Gyre (the region indicated by the green dotted line in Figure 6a) in the periods labeled. The total heat content in the region is indicated at the bottom of each panel. (g) Time series of mean central Beaufort Gyre heat content integrated over the layers 10–30 m (yellow, moving average over 30 days) and 30 m to the depth of $S = 33$ (blue, moving average over 180 days). Dashed lines indicate one standard deviation based on data variance in moving 180-day windows.



where eddies become increasingly important in stabilizing the BG, their generation mechanisms, provenance, and evolution will be key to understand.

Continued sea-ice decline toward an entirely exposed ocean each summer will likely also give rise to reduced meltwater in the BG. In recent years, the BG has experienced excess meltwater originating from multiyear ice, but it is reasonable to anticipate that a seasonally ice-free ocean will lead to a net loss of this local freshwater source. The nature of this transition and its consequences remain unexplored.

The summer waters of the Chukchi Sea will likely experience continued warming as the extent and duration of open water and solar absorption increase. While this might suggest a continued buildup of heat in the BG halocline, it is unclear how the surface-ocean warming (and feedbacks to the local atmospheric forcing) will influence the pathways and dynamics for PSW ventilation of the interior BG. The influence and fate of PSW heat in the BG represent a pressing issue, particularly given this water's capacity to entirely melt the overlying sea ice should it be mixed to the surface. Will its eventual fate be to mix up rapidly under energetic wind forcing (a potential scenario given the possibility of increased wind-energy input to the surface ocean in the absence of a thick, concentrated ice pack), or will its heat be diffused by lateral eddy fluxes or more slowly vertically by weak diffusive fluxes?

Predicting changes in the strength of the BG circulation and its capacity to accumulate freshwater and heat relies on our ability to predict the strength and scale of the two main atmospheric centers of action, the BH and the Icelandic Low. In a warming Arctic, it is unclear which atmospheric circulation patterns or modes may be preferred. For example, will ongoing polar warming lead to an expanded Icelandic Low and a reduced BH (favoring freshwater release), or might the suppression of deep convection in the North Atlantic diminish the strength of the Icelandic Low, allowing for intensification of the BH? Depending on the interplay among this large-scale atmospheric forcing, sea ice, and eddy fluxes, BG freshwater may continue to accumulate or be released to the subpolar North Atlantic, where it may in turn influence atmospheric circulation. Viable climate projections will require understanding the physical forcing and feedbacks as well as the processes that will dominate BG dynamics and structure under continued global warming.

We have focused only on a dominant set of BG physical processes and properties here, but the BG is also characterized by a complex and changing set of biological and chemical processes. For example, the BG is experiencing changes in biological production (e.g., Ardyna & Arrigo 2020), inorganic carbon fluxes (e.g., DeGrandpre et al. 2019), and ocean acidification (e.g., Zhang et al. 2020), and recent measurements have even indicated the presence of microplastics throughout its upper water column (Ross et al. 2021). Studies that examine how the physical processes influence the cycling of carbon, oxygen, nutrients, and other chemical elements will be an essential theme of future research.

8. APPENDIX: DATA SOURCES

BG hydrographic data were collected and made available by the Beaufort Gyre Exploration Project based at the Woods Hole Oceanographic Institution (<https://www.whoi.edu/beaufortgyre>) in collaboration with researchers from Fisheries and Oceans Canada at the Institute of Ocean Sciences; they are available from the project website (<https://www.whoi.edu/website/beaufortgyre/data>) as well as from the National Science Foundation's Arctic Data Center (<https://arcticdata.io>). The Ice-Tethered Profiler data were collected and made available by the Ice-Tethered Profiler program (Krishfield et al. 2008, Toole et al. 2011) based at the Woods Hole Oceanographic Institution (<https://www.whoi.edu/itp>); data are also archived at the National Oceanic and Atmospheric Administration (NOAA) National Centers for Environmental



Information (<https://doi.org/10.7289/v5mw2f7x>). Additional hydrographic data are from the World Ocean Database 2018 (<https://www.ncei.noaa.gov/products/world-ocean-database>), augmented with other publicly available sources. Sea-level-pressure and wind-stress fields were estimated from the National Center for Atmospheric Research (NCAR)/National Centers for Environmental Prediction (NCEP) Reanalysis 6-hourly fields. Arctic dynamic topography/geostrophic currents data were provided by the Centre for Polar Observation and Modelling, University College London (http://www.cpom.ucl.ac.uk/dynamic_topography) (Armitage et al. 2016, 2017). Estimates of radiative fluxes were obtained from the European Centre for Medium-Range Weather Forecasts (ECMWF) ERA-Interim reanalysis twice-daily product obtained from the ECMWF data server (<https://apps.ecmwf.int/datasets>). Sea-ice concentration data are from the NOAA/National Snow and Ice Data Center (NSIDC) Climate Data Record of Passive Microwave Sea Ice Concentration, Version 4 (<https://nsidc.org/data/g02202>) and the Near-Real-Time NOAA/NSIDC Climate Data Record of Passive Microwave Sea Ice Concentration, Version 2 (<https://nsidc.org/data/g10016>) (Meier et al. 2021a,b). Ice-drift speeds are from the Polar Pathfinder Daily 25-km EASE-Grid Sea Ice Motion Vectors, Version 4 (Tschudi et al. 2019).

DISCLOSURE STATEMENT

The authors are not aware of any affiliations, memberships, funding, or financial holdings that might be perceived as affecting the objectivity of this review.

ACKNOWLEDGMENTS

Many recent advances in understanding the BG would not have been possible without Andrey Proshutinsky's vision and leadership of the Beaufort Gyre Exploration Project (<https://www.whoi.edu/beaufortgyre>). We are grateful for his insights and discussions and for preparing some of the data presented here. We also thank Rick Krishfield for providing the fresh-water content estimates. We appreciate the insightful comments and suggestions of an anonymous reviewer. Support was provided by the National Science Foundation Office of Polar Programs.

LITERATURE CITED

- Aagaard K, Carmack EC. 1989. The role of sea ice and other fresh water in the Arctic circulation. *J. Geophys. Res. Oceans* 94:14485–98
- Aagaard K, Roach A, Schumacher J. 1985. On the wind-driven variability of the flow through Bering Strait. *J. Geophys. Res. Oceans* 90:7213–21
- Ardyna M, Arrigo KR. 2020. Phytoplankton dynamics in a changing Arctic Ocean. *Nat. Clim. Change* 10:892–903
- Armitage TW, Manucharyan GE, Petty AA, Kwok R, Thompson AF. 2020. Enhanced eddy activity in the Beaufort Gyre in response to sea ice loss. *Nat. Commun.* 11:761
- Armitage TWK, Bacon S, Ridout AL, Petty AA, Wolbach S, Tsamados M. 2017. Arctic Ocean geostrophic circulation 2003–2014. *Cryosphere* 11:1767–80
- Armitage TWK, Bacon S, Ridout AL, Thomas SF, Aksenov Y, Wingham DJ. 2016. Arctic sea surface height variability and change from satellite radar altimetry and GRACE, 2003–2014. *J. Geophys. Res. Oceans* 121:4303–22
- Boury S, Pickart RS, Odier P, Lin P, Li M, et al. 2020. Whither the Chukchi slope current? *J. Phys. Oceanogr.* 50:1717–32
- Brenner S, Rainville L, Thomson J, Cole S, Lee C. 2021. Comparing observations and parameterizations of ice-ocean drag through an annual cycle across the Beaufort Sea. *J. Geophys. Res. Oceans* 126:e2020JC016977
- Carmack E, Aagaard K, Swift J, Perkin R, McLaughlin F, et al. 1998. Thermohaline transitions. In *Physical Processes in Lakes and Oceans*, ed. J Imberger, pp. 179–86. Washington, DC: Am. Geophys. Union



- Carmack E, Yamamoto-Kawai M, Haine TW, Bacon S, Bluhm BA, et al. 2016. Freshwater and its role in the Arctic marine system: sources, disposition, storage, export, and physical and biogeochemical consequences in the Arctic and global oceans. *J. Geophys. Res. Biogeosci.* 121:675–717
- Coachman LK, Aagaard K. 1966. On the water exchange through Bering Strait. *Limnol. Oceanogr.* 11:44–59
- Cole ST, Stadler J. 2019. Deepening of the winter mixed layer in the Canada Basin, Arctic Ocean over 2006–2017. *J. Geophys. Res. Oceans* 124:4618–30
- Cole ST, Toole JM, Lele R, Timmermans ML, Gallaher SG, et al. 2017. Ice and ocean velocity in the Arctic marginal ice zone: ice roughness and momentum transfer. *Elem. Sci. Anthr.* 5:55
- Corlett WB, Pickart RS. 2017. The Chukchi slope current. *Prog. Oceanogr.* 153:50–65
- Danielson S, Ahkinga O, Ashjian C, Basyuk E, Cooper L, et al. 2020. Manifestation and consequences of warming and altered heat fluxes over the Bering and Chukchi Sea continental shelves. *Deep-Sea Res. II* 177:104781
- Davis PED, Lique C, Johnson HL. 2014. On the link between Arctic sea ice decline and the freshwater content of the Beaufort Gyre: insights from a simple process model. *J. Clim.* 27:8170–84
- DeGrandpre MD, Lai CZ, Timmermans ML, Krishfield RA, Proshutinsky A, Torres D. 2019. Inorganic carbon and $p\text{CO}_2$ variability during ice formation in the Beaufort Gyre of the Canada Basin. *J. Geophys. Res. Oceans* 124:4017–28
- Dewey S, Morison J, Kwok R, Dickinson S, Morison D, Andersen R. 2018. Arctic ice-ocean coupling and gyre equilibration observed with remote sensing. *Geophys. Res. Lett.* 45:1499–508
- Doddridge EW, Meneghello G, Marshall J, Scott J, Lique C. 2019. A three-way balance in the Beaufort Gyre: the ice-ocean governor, wind stress, and eddy diffusivity. *J. Geophys. Res. Oceans* 124:3107–24
- Dosser H, Chanona M, Waterman S, Shibley N, Timmermans ML. 2021. Changes in internal wave-driven mixing across the Arctic Ocean: finescale estimates from an 18-year pan-Arctic record. *Geophys. Res. Lett.* 48:e2020GL091747
- Dukhovskoy D, Johnson M, Proshutinsky A. 2006a. Arctic decadal variability from an idealized atmosphere-ice-ocean model: 1. Model description, calibration, and validation. *J. Geophys. Res. Oceans* 111:C06028
- Dukhovskoy D, Johnson M, Proshutinsky A. 2006b. Arctic decadal variability from an idealized atmosphere-ice-ocean model: 2. simulation of decadal oscillations. *J. Geophys. Res. Oceans* 111:C06029
- Fukumori I, Wang O, Fenty I. 2021. Causal mechanisms of sea level and freshwater content change in the Beaufort Sea. *J. Phys. Oceanogr.* 51:3217–34
- Gong D, Pickart RS. 2015. Summertime circulation in the eastern Chukchi Sea. *Deep-Sea Res. II* 118:18–31
- Grabon JS, Toole JM, Nguyen AT, Krishfield RA. 2021. An analysis of Atlantic water in the Arctic Ocean using the Arctic subpolar gyre state estimate and observations. *Prog. Oceanogr.* 198:102685
- Gudkovich Z. 1961. Relation of the ice drift in the Arctic Basin to ice conditions in the Soviet Arctic seas. *Tr. Okeanogr. Kom. Akad. Nauk SSSR* 11:14–21
- Haine TW, Curry B, Gerdes R, Hansen E, Karcher M, et al. 2015. Arctic freshwater export: status, mechanisms, and prospects. *Glob. Planet. Change* 125:13–35
- Holmes RM, Shiklomanov AI, Suslova A, Tretiakov M, McClelland JW, et al. 2019. River discharge. *Bull. Am. Meteorol. Soc.* 100(9):S161–63
- Jackson JM, Carmack E, McLaughlin F, Allen SE, Ingram R. 2010. Identification, characterization, and change of the near-surface temperature maximum in the Canada Basin, 1993–2008. *J. Geophys. Res. Oceans* 115:C05021
- Jakobson E, Vihma T. 2010. Atmospheric moisture budget in the Arctic based on the ERA-40 reanalysis. *Int. J. Climatol.* 30:2175–94
- Karcher M, Kauker F, Gerdes R, Hunke E, Zhang J. 2007. On the dynamics of Atlantic Water circulation in the Arctic Ocean. *J. Geophys. Res. Oceans* 112:C04S02
- Kenigson JS, Timmermans ML. 2021. Arctic cyclone activity and the Beaufort High. *J. Clim.* 34:4119–27
- Krishfield RA, Proshutinsky A, Tateyama K, Williams WJ, Carmack EC, et al. 2014. Deterioration of perennial sea ice in the Beaufort Gyre from 2003 to 2012 and its impact on the oceanic freshwater cycle. *J. Geophys. Res. Oceans* 119:1271–305
- Krishfield RA, Toole JM, Proshutinsky A, Timmermans ML. 2008. Automated Ice-Tethered Profilers for seawater observations under pack ice in all seasons. *J. Atmos. Ocean. Technol.* 25:2091–105



- Kwok R, Morison J. 2011. Dynamic topography of the ice-covered Arctic Ocean from ICESat. *Geophys. Res. Lett.* 38:L02501
- Kwok R, Rothrock D. 2009. Decline in Arctic sea ice thickness from submarine and ICESat records: 1958–2008. *Geophys. Res. Lett.* 36:L15501
- Lin P, Pickart RS, Våge K, Li J. 2021. Fate of warm Pacific water in the Arctic basin. *Geophys. Res. Lett.* 48:e2021GL094693
- Liu Z, Risi C, Codron F, He X, Poulsen CJ, et al. 2021. Acceleration of western Arctic sea ice loss linked to the Pacific North American pattern. *Nat. Commun.* 12:1519
- Manucharyan GE, Spall MA, Thompson AF. 2016. A theory of the wind-driven Beaufort Gyre variability. *J. Phys. Oceanogr.* 46:3263–78
- Martin T, Steele M, Zhang J. 2014. Seasonality and long-term trend of Arctic Ocean surface stress in a model. *J. Geophys. Res. Oceans* 119:1723–38
- Maykut G, McPhee MG. 1995. Solar heating of the Arctic mixed layer. *J. Geophys. Res. Oceans* 100:24691–703
- McPhee MG. 2013. Intensification of geostrophic currents in the Canada Basin, Arctic Ocean. *J. Clim.* 26:3130–38
- Meier W, Fetterer F, Windnagel AK, Stewart JS. 2021a. *Near-real-time NOAA/NSIDC climate data record of passive microwave sea ice concentration, version 2*. Data Set G10016, Natl. Snow Ice Data Cent., Boulder, CO. <https://nsidc.org/data/G10016/versions/2>
- Meier W, Fetterer F, Windnagel AK, Stewart JS. 2021b. *NOAA/NSIDC climate data record of passive microwave sea ice concentration, version 4*. Data Set G02202, Natl. Snow Ice Data Cent., Boulder, CO. <https://nsidc.org/data/G02202/versions/4>
- Meier W, Perovich D, Farrell S, Haas C, Hendricks S, et al. 2021c. Sea ice. *Bull. Am. Meteorol. Soc.* 102(8):S279–82
- Meneghello G, Marshall J, Cole ST, Timmermans ML. 2017. Observational inferences of lateral eddy diffusivity in the halocline of the Beaufort Gyre. *Geophys. Res. Lett.* 44:12331–38
- Meneghello G, Marshall J, Lique C, Isachsen PE, Doddridge E, et al. 2021. Genesis and decay of mesoscale baroclinic eddies in the seasonally ice-covered interior Arctic Ocean. *J. Phys. Oceanogr.* 51:115–29
- Meneghello G, Marshall J, Timmermans ML, Scott J. 2018. Observations of seasonal upwelling and downwelling in the Beaufort Sea mediated by sea ice. *J. Phys. Oceanogr.* 48:795–805
- Moore G, Schweiger A, Zhang J, Steele M. 2018. Collapse of the 2017 winter Beaufort High: a response to thinning sea ice? *Geophys. Res. Lett.* 45:2860–69
- Morison J, Kwok R, Dickinson S, Andersen R, Peralta-Ferriz C, et al. 2021. The cyclonic mode of Arctic Ocean circulation. *J. Phys. Oceanogr.* 51:1053–75
- Morison J, Kwok R, Peralta-Ferriz C, Alkire M, Rigor I, et al. 2012. Changing Arctic Ocean freshwater pathways. *Nature* 481:66–70
- Morison J, Steele M, Andersen R. 1998. Hydrography of the upper Arctic Ocean measured from the nuclear submarine USS *Pargo*. *Deep-Sea Res. I* 45:15–38
- Overland JE, Adams JM, Bond NA. 1999. Decadal variability of the Aleutian Low and its relation to high-latitude circulation. *J. Clim.* 12:1542–48
- Padman L, Dillon TM. 1987. Vertical heat fluxes through the Beaufort Sea thermohaline staircase. *J. Geophys. Res. Oceans* 92:10799–806
- Peralta-Ferriz C, Woodgate RA. 2015. Seasonal and interannual variability of pan-Arctic surface mixed layer properties from 1979 to 2012 from hydrographic data, and the dominance of stratification for multiyear mixed layer depth shoaling. *Prog. Oceanogr.* 134:19–53
- Perovich DK, Light B, Eicken H, Jones KF, Runciman K, Nghiem SV. 2007. Increasing solar heating of the Arctic Ocean and adjacent seas, 1979–2005: attribution and role in the ice-albedo feedback. *Geophys. Res. Lett.* 34:L19505
- Perovich DK, Richter-Menge JA. 2009. Loss of sea ice in the Arctic. *Annu. Rev. Mar. Sci.* 1:417–41
- Pisareva MN, Pickart RS, Lin P, Fratantoni PS, Weingartner TJ. 2019. On the nature of wind-forced upwelling in Barrow Canyon. *Deep-Sea Res. II* 162:63–78
- Proshutinsky A, Bourke RH, McLaughlin FA. 2002. The role of the Beaufort Gyre in Arctic climate variability: seasonal to decadal climate scales. *Geophys. Res. Lett.* 29:15-1–4



- Proshutinsky A, Dukhovskoy D, Timmermans ML, Krishfield RA, Bamber JL. 2015. Arctic circulation regimes. *Philos. Trans. R. Soc. A* 373:20140160
- Proshutinsky A, Johnson MA. 1997. Two circulation regimes of the wind-driven Arctic Ocean. *J. Geophys. Res. Oceans* 102:12493–514
- Proshutinsky A, Krishfield RA, Timmermans ML. 2020. Introduction to special collection on Arctic Ocean Modeling and Observational Synthesis (FAMOS) 2: Beaufort Gyre phenomenon. *J. Geophys. Res. Oceans* 125:e2019JC015400
- Proshutinsky A, Krishfield RA, Timmermans ML, Toole JM, Carmack E, et al. 2009. Beaufort Gyre freshwater reservoir: state and variability from observations. *J. Geophys. Res.* 114:C00A10
- Proshutinsky A, Krishfield RA, Toole JM, Timmermans ML, Williams W, et al. 2019. Analysis of the Beaufort Gyre freshwater content in 2003–2018. *J. Geophys. Res. Oceans* 124:9658–89
- Regan HC, Lique C, Armitage TW. 2019. The Beaufort Gyre extent, shape, and location between 2003 and 2014 from satellite observations. *J. Geophys. Res. Oceans* 124:844–62
- Rigor IG, Wallace JM, Colony RL. 2002. Response of sea ice to the Arctic Oscillation. *J. Clim.* 15:2648–63
- Rosenblum E, Fajber R, Stroeve JC, Gille ST, Tremblay LB, Carmack EC. 2021. Surface salinity under transitioning ice cover in the Canada Basin: climate model biases linked to vertical distribution of fresh water. *Geophys. Res. Lett.* 48:e2021GL094739
- Ross PS, Chastain S, Vassilenko E, Etemadifar A, Zimmermann S, et al. 2021. Pervasive distribution of polyester fibres in the Arctic Ocean is driven by Atlantic inputs. *Nat. Commun.* 12:106
- Schauer U, Losch M. 2019. “Freshwater” in the ocean is not a useful parameter in climate research. *J. Phys. Oceanogr.* 49:2309–21
- Schweiger A, Lindsay R, Zhang J, Steele M, Stern H, Kwok R. 2011. Uncertainty in modeled Arctic sea ice volume. *J. Geophys. Res. Oceans* 116:C00D06
- Serreze MC, Barrett AP. 2011. Characteristics of the Beaufort Sea high. *J. Clim.* 24:159–82
- Serreze MC, Barry RG. 2014. *The Arctic Climate System*. Cambridge, UK: Cambridge Univ. Press
- Serreze MC, Carse F, Barry RG, Rogers JC. 1997. Icelandic Low cyclone activity: climatological features, linkages with the NAO, and relationships with recent changes in the Northern Hemisphere circulation. *J. Clim.* 10:453–64
- Serreze MC, Meier WN. 2019. The Arctic’s sea ice cover: trends, variability, predictability, and comparisons to the Antarctic. *Ann. N.Y. Acad. Sci.* 1436:36–53
- Shaw WJ, Stanton TP. 2014. Vertical diffusivity of the Western Arctic Ocean halocline. *J. Geophys. Res. Oceans* 119:5017–38
- Shimada K, Itoh M, Nishino S, McLaughlin F, Carmack E, Proshutinsky A. 2005. Halocline structure in the Canada Basin of the Arctic Ocean. *Geophys. Res. Lett.* 32:L03606
- Sokolov AL. 1966. Drift of ice in the Arctic basin and changes in ice conditions over the northern sea route. *Probl. Arct. Anarct.* 11:1–20
- Spall MA. 2007. Circulation and water mass transformation in a model of the Chukchi Sea. *J. Geophys. Res. Oceans* 112:C05025
- Spall MA, Pickart RS, Fratantoni PS, Plueddemann AJ. 2008. Western Arctic shelfbreak eddies: formation and transport. *J. Phys. Oceanogr.* 38:1644–68
- Spreen G, de Steur L, Divine D, Gerland S, Hansen E, Kwok R. 2020. Arctic sea ice volume export through Fram Strait from 1992 to 2014. *J. Geophys. Res. Oceans* 125:e2019JC016039
- Steele M, Zhang J, Ermold W. 2010. Mechanisms of summertime upper Arctic Ocean warming and the effect on sea ice melt. *J. Geophys. Res. Oceans* 115:C11004
- Thompson DW, Wallace JM. 1998. The Arctic Oscillation signature in the wintertime geopotential height and temperature fields. *Geophys. Res. Lett.* 25:1297–300
- Timmermans ML. 2015. The impact of stored solar heat on Arctic sea ice growth. *Geophys. Res. Lett.* 42:3944–406
- Timmermans ML, Marshall J. 2020. Understanding Arctic Ocean circulation: a review of ocean dynamics in a changing climate. *J. Geophys. Res. Oceans* 125:e2018JC014378
- Timmermans ML, Marshall J, Proshutinsky A, Scott J. 2017. Seasonally derived components of the Canada Basin halocline. *Geophys. Res. Lett.* 44:5008–15



- Timmermans ML, Proshutinsky A, Golubeva E, Jackson JM, Krishfield RA, et al. 2014. Mechanisms of Pacific Summer Water variability in the Arctic's central Canada Basin. *J. Geophys. Res. Oceans* 119:7523–48
- Timmermans ML, Proshutinsky A, Krishfield RA, Perovich DK, Richter-Menge JA, et al. 2011. Surface freshening in the Arctic Ocean's Eurasian Basin: an apparent consequence of recent change in the wind-driven circulation. *J. Geophys. Res. Oceans* 116:C00D03
- Timmermans ML, Toole JM, Krishfield RA. 2018. Warming of the interior Arctic Ocean linked to sea ice losses at the basin margins. *Sci. Adv.* 4:eaat6773
- Toole JM, Krishfield RA, Timmermans ML, Proshutinsky A. 2011. The Ice-Tethered Profiler: Argo of the Arctic. *Oceanography* 24(3):126–35
- Toole JM, Timmermans ML, Perovich DK, Krishfield RA, Proshutinsky A, Richter-Menge JA. 2010. Influences of the ocean surface mixed layer and thermohaline stratification on Arctic sea ice in the central Canada Basin. *J. Geophys. Res. Oceans* 115:C10018
- Tschudi M, Meier W, Stewart J, Fowler C, Maslanik J. 2019. *Polar Pathfinder daily 25 km EASE-grid sea ice motion vectors, version 4*. Data Set NSIDC-0116, Natl. Snow Ice Data Cent., Boulder, CO. <https://nsidc.org/data/NSIDC-0116/versions/4>
- Vellinga M, Dickson B, Curry R. 2008. The changing view on how freshwater impacts the Atlantic Meridional Overturning Circulation. In *Arctic-Subarctic Ocean Fluxes: Defining the Role of the Northern Seas in Climate*, ed. RR Dickson, J Meincke, P Rhines, pp. 289–313. Dordrecht, Neth.: Springer
- Vihma T, Screen J, Tjernström M, Newton B, Zhang X, et al. 2016. The atmospheric role in the Arctic water cycle: a review on processes, past and future changes, and their impacts. *J. Geophys. Res. Biogeosci.* 121:586–620
- Weingartner TJ, Cavalieri DJ, Aagaard K, Sasaki Y. 1998. Circulation, dense water formation, and outflow on the northeast Chukchi shelf. *J. Geophys. Res. Oceans* 103:7647–61
- Weingartner TJ, Potter RA, Stouff CA, Dobbins EL, Stascewich H, et al. 2017. Transport and thermohaline variability in Barrow Canyon on the Northeastern Chukchi Sea Shelf. *J. Geophys. Res. Oceans* 122:3565–85
- Williams WJ, Shroyer E, Clement Kinney J, Itoh M, Maslowski W. 2014. Shelf-break exchange in the Bering, Chukchi and Beaufort Seas. In *The Pacific Arctic Region*, ed. J Grebmeier, W Maslowski, pp. 133–65. Dordrecht, Neth.: Springer
- Winsor P, Björk G. 2000. Polynya activity in the Arctic Ocean from 1958 to 1997. *J. Geophys. Res. Oceans* 105:8789–803
- Winsor P, Chapman DC. 2002. Distribution and interannual variability of dense water production from coastal polynyas on the Chukchi shelf. *J. Geophys. Res. Oceans* 107:16–1–15
- Woodgate RA, Aagaard K, Weingartner TJ. 2005. Monthly temperature, salinity, and transport variability of the Bering Strait through flow. *Geophys. Res. Lett.* 32:L04601
- Woodgate RA, Peralta-Ferriz C. 2021. Warming and freshening of the Pacific inflow to the Arctic from 1990–2019 implying dramatic shoaling in Pacific Winter Water ventilation of the Arctic water column. *Geophys. Res. Lett.* 48:e2021GL092528
- Woodgate RA, Weingartner T, Lindsay R. 2010. The 2007 Bering Strait oceanic heat flux and anomalous Arctic sea-ice retreat. *Geophys. Res. Lett.* 37:L01602
- Zhang J, Weijer W, Steele M, Cheng W, Verma T, Veneziani M. 2021. Labrador Sea freshening linked to Beaufort Gyre freshwater release. *Nat. Commun.* 12:1229
- Zhang M, Perrie W, Long Z. 2019. Decadal variations in the winter Beaufort High and the stratospheric polar vortex. *Geophys. Res. Lett.* 46:4933–41
- Zhang Y, Yamamoto-Kawai M, Williams W. 2020. Two decades of ocean acidification in the surface waters of the Beaufort Gyre, Arctic Ocean: effects of sea ice melt and retreat from 1997–2016. *Geophys. Res. Lett.* 47:e60119
- Zhao M, Timmermans ML. 2015. Vertical scales and dynamics of eddies in the Arctic Ocean's Canada Basin. *J. Geophys. Res. Oceans* 120:8195–209
- Zhao M, Timmermans ML, Cole S, Krishfield RA, Toole JM. 2016. Evolution of the eddy field in the Arctic Ocean's Canada Basin, 2005–2015. *Geophys. Res. Lett.* 43:8106–14
- Zhao M, Timmermans ML, Krishfield RA, Manucharyan G. 2018. Partitioning of kinetic energy in the Arctic Ocean's Beaufort Gyre. *J. Geophys. Res. Oceans* 123:4806–19

